Journal of Nanopores Systems

Original Research Paper

Process Modeling of Methylene blue Removal Using Fe/Quasi MOF UIO-66 (Zr) Nanocomposite based on GMDH Neural Network

Ali Safari*, Farhad Heidary

Department of Chemistry, Faculty of Science, Arak University, Arak 3848177584, Iran

Article history
Received: 9 June 2026
Revised: 23 June 2026
Accepted: 25 June 2026

*Corresponding Author:
Ali Safari
Department of Chemistry, Faculty of Science, Arak University, Arak 3848177584, Iran
Email: alisafari3081376@gmail.com

Abstract: In this study, Fe/Quasi MOF UIO-66 (Zr) nanocomposite was synthesized via an ultrasonic method and characterized using XRD, FTIR, SEM, and N_2 physisorption analysis. The adsorption performance for methylene blue removal from aqueous solution was evaluated under varying parameters including adsorbent dosage (5-45 mg), pH (3-11), initial dye concentration (10^{-5}-10^{-9} M), contact time (3-20 min), and temperature (25-80 °C). Experimental optimization revealed that maximum removal efficiency (>96%) was achieved at 45 mg adsorbent, pH 11, initial concentration 10^{-9} M, time 12 min, and temperature 70 °C. The core innovation of this work lies in the development of a GMDH (Group Method of Data Handling) neural network combined with a genetic algorithm to model the removal process. The optimized model predicted residual dye concentration with high accuracy (test RMSE = 0.00684, R^2 = 0.9922). Sensitivity analysis based on input variable frequency in the optimal chromosome revealed that adsorbent dosage (8 repeats), pH (7 repeats), and contact time (7 repeats) exerted the greatest influence on process performance. The proposed modeling approach offers a reliable analytical tool for predicting and optimizing wastewater treatment processes without extensive experimentation.

Keywords: Nanocomposite, Quasi metal-organic framework, Methylene blue removal, GMDH modeling, Sensitivity analysis

Introduction

Freshwater scarcity has emerged as one of the most pressing global challenges of the 21st century. Although water covers approximately 71% of the Earth‘s surface, only 2.5% is freshwater, and merely a fraction of this is accessible for human use [1]. Rapid industrialization, population growth, and agricultural expansion have significantly exacerbated water pollution, with industrial wastewater containing persistent organic pollutants posing a particularly severe threat to aquatic ecosystems and public health [2,3].

Synthetic dyes represent a major category of environmental contaminants. These compounds are extensively employed in textile manufacturing, leather processing, paper production, food industries, and pharmaceutical sectors due to their cost-effectiveness, color variety, and ease of application [4-6]. Methylene blue, a representative cationic thiazine dye, is widely used in textile dyeing and biomedical applications; its discharge into water bodies reduces light penetration, inhibits photosynthesis, and poses carcinogenic and mutagenic risks to aquatic organisms and human health [7,8].

Conventional wastewater treatment methods, including coagulation, flocculation, membrane filtration, and biological treatment, often suffer from limitations such as incomplete pollutant removal, high operational costs, secondary sludge generation, and

sensitivity to fluctuating operating conditions [9,10]. Consequently, advanced oxidation processes (AOPs) and heterogeneous catalysis have gained increasing attention as promising alternatives for complete mineralization of recalcitrant organic pollutants [11].

Metal-organic frameworks (MOFs) have emerged as a class of highly porous crystalline materials composed of metal ions or clusters interconnected by organic linkers [12]. Their exceptional properties—including ultrahigh specific surface area, tunable pore architecture, structural diversity, and tailorable surface chemistry—render them ideal candidates for adsorption, separation, and catalytic applications [13,14]. Among thousands of reported MOF structures, UIO-66 (Zr) stands out due to its extraordinary chemical and thermal stability, arising from the strong coordination bonds between Zr(IV) nodes and carboxylate ligands of terephthalic acid [15]. This stability enables UIO-66 to maintain structural integrity under harsh conditions, including exposure to acidic or basic media and elevated temperatures [16].

Incorporation of transition metals such as iron into MOF frameworks has been demonstrated to enhance catalytic activity by introducing additional active sites and promoting electron transfer processes [17]. Furthermore, controlled thermal treatment of MOFs produces quasi-MOF structures, wherein partial removal of organic ligands creates unsaturated metal sites and positively charged vacancies that significantly improve adsorption performance [18]. These defect-engineered structures exhibit enhanced Lewis acidity, increased accessibility of active centers, and improved charge separation efficiency [19,20].

Recent studies have increasingly focused on the application of MOF-based adsorbents for the removal of cationic dyes from aqueous media. For instance, Wang et al. (2021) demonstrated that UiO-66-based MOFs exhibit promising photocatalytic activity for dye degradation under simulated solar irradiation. Moreover, iron-modified MOFs have attracted considerable attention due to their enhanced adsorption capacity and magnetic recoverability [17]. Wan et al. (2024) reported that defect-engineered Fe-MOFs could achieve over 90% removal of methylene blue within 30 minutes through a combined adsorption-photocatalysis mechanism [21]. Similarly, Hemdan et al. (2024) developed a sodium alginate-encapsulated nano-iron oxide coupled with Cu-based MOFs for effective dye removal [22]. These findings highlight the potential of Fe-modified quasi-MOF structures as efficient adsorbents for wastewater treatment.

While numerous experimental studies have investigated dye removal using MOF-based catalysts, relatively few have employed artificial intelligence-based approaches for process modeling and prediction. The Group Method of Data Handling (GMDH) is a self-organizing neural network that automatically selects optimal model structures and identifies nonlinear relationships between input and output variables without requiring prior assumptions about the underlying mathematical form [23]. GMDH has been successfully applied for modeling complex chemical processes, including dye removal from aqueous solutions [22], where it demonstrated superior predictive capability compared to conventional regression methods. The integration of genetic algorithms with GMDH further enhances model optimization by efficiently searching for optimal network architectures [24].

The objectives of the present study are threefold: (i) synthesis and comprehensive characterization of Fe/Quasi MOF UIO-66 (Zr) nanocomposite; (ii) experimental optimization of methylene blue removal parameters including adsorbent dosage, pH, initial dye concentration, contact time, and temperature; and (iii) development of a GMDH-GA hybrid model for predicting removal efficiency and identifying the most influential parameters through rigorous sensitivity analysis.

Materials and Methods

Chemicals

All chemicals were purchased from reputable suppliers (Merck, Germany; Sigma-Aldrich, USA; Razi, Iran) with the purity of exceeding 98% and used without further purification. The following reagents were employed: zirconium chloride ($ZrCl_4$, 99%), 1,4-benzenedicarboxylic acid (BDC, 99%), N,N-dimethylformamide (DMF, 99%), iron(III) nitrate nonahydrate ($Fe(NO_3)_3 \cdot 9H_2O$, 99%), ethanol (96%), hydrochloric acid (HCl, 37%), sodium hydroxide (NaOH, 99%), and methylene blue ($C_{16}H_{18}ClN_3S$, 98%). Deionized water with conductivity below 1 μS/cm was prepared using a Zolab water purification system.

Characterization

The crystalline structure of the synthesized nanocomposite was analyzed using X-ray diffraction (XRD; Philips X'Pert) with Cu-Kα radiation (λ = 1.5418 Å) operating at 40 kV and 30 mA, with 2θ ranging from 5° to 70° at a scan rate of $2° \cdot min^{-1}$. The average crystallite size was calculated using the Scherrer equation: $\tau = k\lambda/(\beta \cos\theta)$, where k is the shape factor (0.9), λ is the X-ray wavelength, β is the full width at half maximum (FWHM), and θ is the Bragg angle [25].

Fourier transform infrared (FTIR) spectra were recorded on a Bruker Tensor 27 spectrometer in the range of 400–4000 cm^{-1} using the KBr pellet technique, with 32 scans at a resolution of 4 cm^{-1}.

Surface morphology was examined using field emission scanning electron microscopy (FE-SEM; TESCAN MIRA3) with an accelerating voltage of 15 kV. Samples were sputter-coated with gold prior to analysis.

Specific surface area and porosity were determined by nitrogen adsorption-desorption isotherms at 77 K using a Micromeritics ASAP 2020 analyzer. The specific surface area was determined by N_2 physisorption analysis and calculated using the BET method from the adsorption branch in the relative pressure range $P/P_0 = 0.05–0.30$, and pore size distribution was determined using the BJH (Barrett-Joyner-Halenda) method.

Synthesis of Fe/Quasi MOF UIO-66 (Zr) Nanocomposite

The synthesis procedure followed a modified protocol based on previous reports [26]. In a typical synthesis, 10 mL DMF, 0.125 g $ZrCl_4$, and 1 mL HCl were mixed in a beaker with magnetic stirring for 20 s. Separately, 5 mL DMF and 0.123 g BDC were dissolved in another beaker. Then, 5 mL of 1 M $Fe(NO_3)_3$ solution was added to the first beaker to incorporate iron species into the framework. The contents of both beakers were combined and subjected to ultrasonic treatment in an ultrasonic bath (100 W, 40 kHz) for 20 min to ensure homogeneous mixing.

The resulting solution (approximately 15 mL) was transferred into glass vials and placed in an oven at 80 °C for 24 h to promote crystallization. After the reaction, the precipitate was separated by centrifugation at 2500 rpm for 10 min, washed twice with DMF and twice with absolute ethanol to remove unreacted precursors and solvent residues, and subsequently dried at 100 °C for 24 h.

To obtain the quasi-MOF structure, the as-synthesized material was calcined in a muffle furnace at 350 °C for 15 min with a heating rate of 5 °C·min^{-1} under ambient atmosphere. This thermal treatment selectively removes a fraction of organic ligands, generating unsaturated metal sites and positively charged vacancies that enhance adsorption activity.

Removal Experiments

Methylene blue stock solutions were prepared at concentrations of 10^{-5}, 10^{-6}, 10^{-7}, 10^{-8}, and 10^{-9} M by serial dilution of a 10^{-3} M stock solution in deionized water. The pH of the dye solutions was adjusted to desired values (3, 5, 7, 9, and 11) using 0.1 M HCl or 0.1 M NaOH solutions, measured with a calibrated pH meter.

In each removal experiment, a specified amount of Fe/Quasi MOF UIO-66 (Zr) adsorbent (5, 10, 15, 20, 25, 30, 35, 40, or 45 mg) was added to 10 mL of methylene blue solution in a 50 mL Erlenmeyer flask. The mixture was agitated on a magnetic stirrer at 300 rpm under controlled temperature (30, 50, 70, or 80 °C) using a thermostated water bath. After predetermined contact times (3, 5, 7, 10, 12, 15, 18, or 20 min), the adsorbent was separated by centrifugation at 4000 rpm for 5 min. The residual dye concentration in the supernatant was analyzed using a UV-Vis spectrophotometer (Shimadzu UV-1800) at the maximum absorption wavelength of methylene blue (λ = 664 nm).

The removal efficiency (%) was calculated using the following equation:

$$\% \text{ Removal} = \frac{C_0 - C_t}{C_0} \times 100 \qquad (1)$$

where C_0 (mg·L^{-1}) represents the initial dye concentration and C_t (mg·L^{-1}) represents the residual dye concentration at time t (min). All experiments were repeated independently, and the reported values correspond to averaged measurements.

Results and Discussions

X-ray Diffraction Patterns

The X-ray diffraction pattern of the synthesized Fe/Quasi MOF UIO-66 (Zr) nanocomposite is presented in Fig. 1. Characteristic peaks were observed at 2θ values of approximately 8.5°, 25.7° and 30.1°, which correspond well to the simulated pattern of UIO-66 reported in the literature [27,28]. A weak reflection associated with the UiO-66 framework is expected around 7.4°, although its intensity is relatively low in the present sample after Fe incorporation and thermal treatment. The preservation of the main diffraction peaks after iron doping and thermal treatment confirms that the crystalline framework structure of UIO-66 remained intact. The absence of additional peaks corresponding to iron oxide phases suggests that iron species were successfully incorporated into the MOF framework rather than forming separate crystalline domains.

The average crystallite size was calculated using the Scherrer equation based on the most intense peak at 2θ = 8.5°. The calculated value of 73 nm confirms the nanoscale nature of the synthesized material, consistent with the typical particle size range of MOF-based nanomaterials [29].

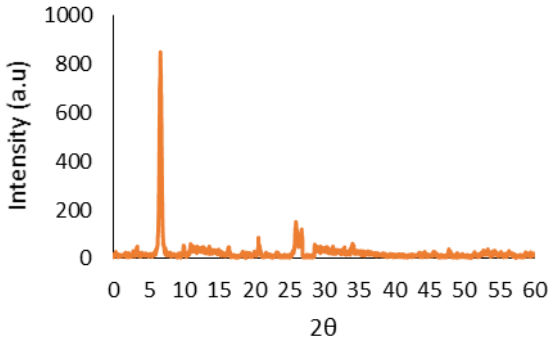

Fig. 1. XRD spectrum for synthetic adsorbent.

FT-IR Analysis

The FTIR spectrum of Fe/Quasi MOF UiO-66 (Fig. 2b) exhibits several characteristic absorption bands. A broad band centered at 3400 cm^{-1} is assigned to O–H stretching vibrations of adsorbed water and surface hydroxyl groups. The strong bands at 1590 and 1395 cm^{-1} correspond to the asymmetric and symmetric stretching vibrations of the carboxylate groups ($–COO^–$) coordinated to Zr(IV) clusters, confirming successful linker coordination [30]. The weak shoulder at around 1700 cm^{-1}, which appears only in the quasi-MOF sample (Fig. 2b), indicates the presence of free carboxylic acid groups resulting from partial decarboxylation during thermal treatment. Bands in the region of 400–600 cm^{-1} are attributed to Fe–O and Zr–O stretching vibrations [31]. The absence of a carbonyl band near 1720 cm^{-1} in the pristine MOF (Fig. 2a) confirms complete deprotonation of the BDC linkers.

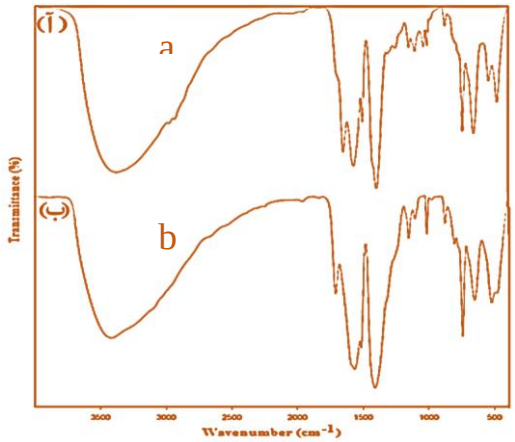

Fig. 2. FTIR spectrum for (a) MOF UiO-66 and (b) e/Quasi MOF UiO-66

SEM Morphology

The SEM images confirm the formation of nanoscale aggregated particles. The particle size estimated from SEM observations is generally consistent with the crystallite size calculated from XRD analysis, although precise particle size determination was not performed from the SEM images (fig. 3).

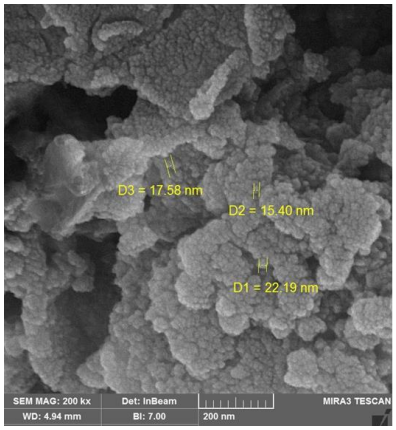

Fig. 3. SEM image of the synthetic sample

N_2 physisorption analysis Surface Area and Porosity

The specific surface area was determined by N_2 physisorption analysis and was found to be 314.5 $m^2 \cdot g^{-1}$, with a pore volume of 0.198 $cm^3 \cdot g^{-1}$ and an average pore diameter of 14.46 nm (Table 1). These values are reasonable for a quasi-MOF material following calcination at 350 °C, which removes a portion of organic linkers and generates additional porosity. The surface area is comparable to values reported for defect-engineered Fe-MOFs intended for dye removal applications. The nitrogen adsorption-desorption isotherm of the Fe/Quasi MOF UIO-66 nanocomposite exhibited a Type IV isotherm with an H2-type hysteresis loop (Fig. 4), characteristic of mesoporous materials [21].

Table 1. The results of measuring the surface properties of the adsorbent by N_2 physisorption analysis

Name	Average pore size (nm)	Specific Area (m^2/g)	Specific Volume (cm^3/g)
Fe/Quasi MOF	14.46	314.5	0.198

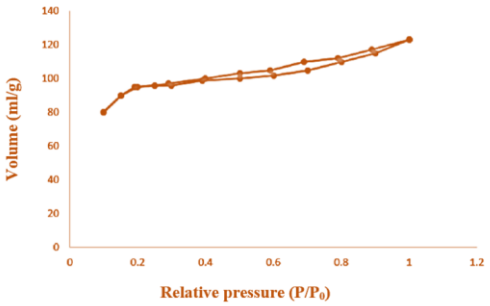

Fig. 4. N_2 adsorption-desorption isotherm for Fe/Quasi MOF

GMDH Neural Network Modeling

The Group Method of Data Handling (GMDH) is a self-organizing neural network that automatically identifies the optimal model structure by generating and evaluating successive layers of polynomial neurons [32]. Unlike conventional neural networks that require predetermined architectures, GMDH constructs the network incrementally, selecting only the most informative neurons at each layer.

In this study, a GMDH-GA hybrid approach was implemented for modeling the methylene blue removal process. The model considered five input variables: pH (X_1), adsorbent dosage in grams (X_2), logarithm of initial dye concentration (X_3), temperature in °C (X_4), and contact time in minutes (X_5). The output variable was the residual dye concentration (C_t) in M.

The experimental dataset comprised 34 data points, which were randomly partitioned into training (26 points, 76.5%) and testing (8 points, 23.5%) subsets. The training set was used for model construction, while the testing set served for model validation.

The GMDH algorithm operates as follows:

1. In the first layer, all possible pairwise combinations of the five input variables were generated (10 combinations).
2. For each combination, a quadratic polynomial neuron of the form $y = a + bx_i + cx_j + dx_i^2 + ex_j^2 + fx_ix_j$ was trained using ordinary least squares regression.
3. The root mean square error (RMSE) was calculated for each neuron on the validation subset.
4. Neurons with the lowest RMSE values were selected and passed to the next layer as new input variables.
5. This iterative process continued until no further reduction in prediction error was achieved or a maximum of five layers was reached.

A genetic algorithm (GA) was integrated with the GMDH framework to optimize the model architecture. The GA parameters were: population size 50, 200 generations, crossover probability 0.8, mutation probability 0.01, and tournament selection. The objective function minimized the RMSE on the testing dataset.

Model performance was evaluated using the following statistical metrics:

$$\mathrm{RMSE} = \sqrt{\frac{1}{n}\sum_{i=1}^{n}(y_i - \hat{y}_i)^2} \qquad (2)$$

$$R^2 = 1 - \frac{\sum_{i=1}^{n}(y_i - \hat{y}_i)^2}{\sum_{i=1}^{n}(y_i - \bar{y})^2} \qquad (3)$$

where y_i, $\hat{y}_i$, and $\bar{y}$ represent experimental values, predicted values, and mean experimental values, respectively, and n is the number of data points.

Sensitivity analysis was performed by counting the frequency of each input variable appearing in the first-layer neurons of the optimal chromosome [33]. Variables with higher frequencies were considered to exert greater influence on the removal process.

Optimization of removal Parameters

Effect of adsorbent Dosage

The influence of Fe/Quasi MOF UIO-66 (Zr) dosage on methylene blue removal efficiency was investigated over the range of 5-45 mg under fixed conditions (pH 7, initial dye concentration 10^{-5} M, contact time 10 min, temperature 25 °C). As shown in Fig. 5, increasing the adsorbent dosage from 5 to 45 mg resulted in a progressive increase in removal efficiency from 42% to 96%. This positive correlation is attributed to the greater availability of active sites at higher adsorbent loadings, which enhances the probability of dye molecule adsorption and subsequent removal. An adsorbent dosage of 45 mg was selected as the optimal value for subsequent experiments, as further increases were not practical due to handling limitations and potential light scattering effects.

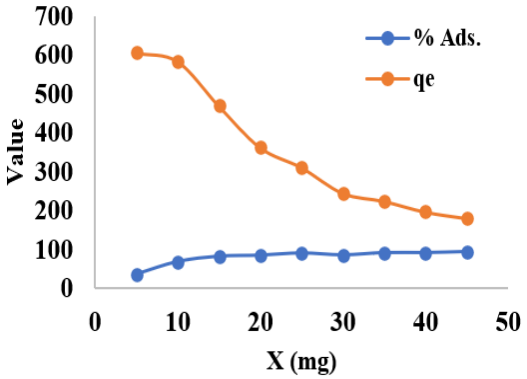

Fig. 5. The effect of different amounts of adsorbent on dye removal from aqueous solution.

Effect of Contact Time

The time-dependent removal profile (Fig. 6) was examined under optimized adsorbent dosage (45 mg) with other parameters maintained constant. removal efficiency increased rapidly during the initial 12 minutes, reaching 94.5%, and then exhibited a slight decrease to approximately 92% at 20 minutes. The initial rapid phase reflects the abundance of vacant active sites and the high concentration gradient driving dye molecules toward the adsorbent surface. The subsequent slight decline may be attributed to saturation of active sites coupled with a partial desorption of adsorbed dye molecules back into the aqueous phase. A contact time of 12 minutes was selected as optimal.

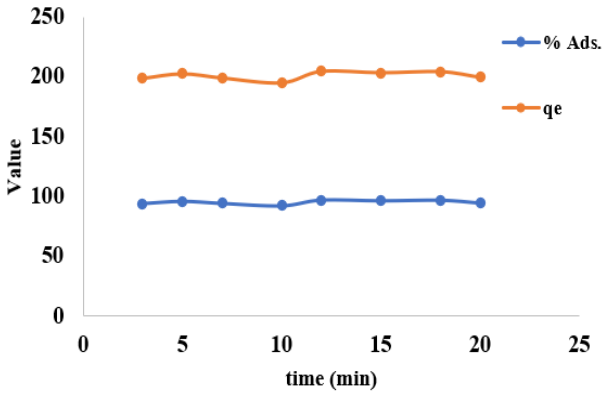

Fig. 6. The effect of different contact times on dye removal from aqueous solution.

Effect of pH

The solution pH plays a critical role in determining both the surface charge of the adsorbent and the ionization state of the dye molecules. The effect of initial pH in the range of 3-11 was evaluated under optimal adsorbent dosage and contact time conditions (Fig. 7). Removal efficiency increased from 45% at pH 3 to 72% at pH 7 and further to 97% at pH 11. This marked enhancement under alkaline conditions can be rationalized as follows: (i) the improved removal efficiency at alkaline pH is mainly attributed to enhanced electroststic attraction between methylene blue molecules and negatively charged adsorption sites; (ii) the positively charged methylene blue molecules exhibit enhanced electrostatic attraction to deprotonated surface hydroxyl groups on the adsorbent under basic conditions.

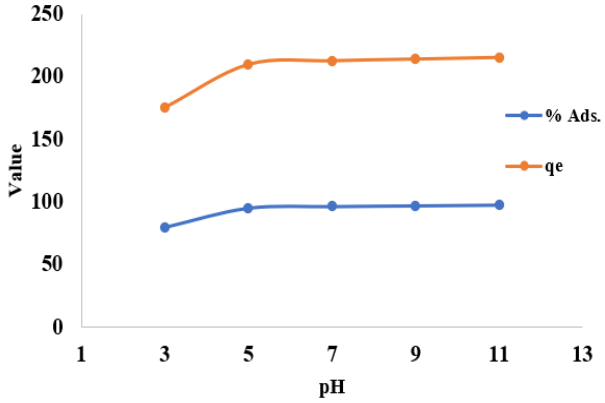

Fig. 7. The effect of different pH on dye removal from aqueous solution.

Effect of Temperature

Removal experiments were conducted at temperatures ranging from 30 to 80 °C (Fig. 8). Increasing the temperature from 30 to 70 °C enhanced removal efficiency from 89% to 95%, indicating that the removal process is endothermic in nature. This temperature dependence suggests that higher temperatures cause to increase the collision frequency between dye molecules and active sites, facilitate diffusion of dye molecules toward adsorption sites. However, at 80 °C, the efficiency decreased slightly to 93%, possibly due to partial deactivation of active sites, increased molecular mobility leading to desorption, or minor structural changes in the adsorbent at elevated temperatures. Based on these results, 70 °C was selected as the optimal temperature.

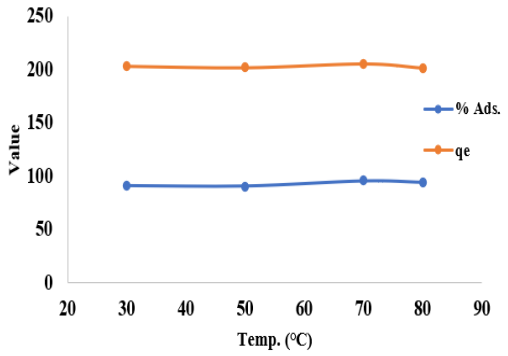

Fig. 8. The effect of different temperatures on dye removal from aqueous solution.

Effect of Initial Dye Concentration

The influence of initial methylene blue concentration was examined across the range of 10^{-5} to 10^{-9} M under otherwise optimal conditions (Fig. 9). Contrary to typical adsorption processes where higher initial concentrations yield higher absolute removal amounts but lower percentage removal, in this study removal efficiency increased as initial concentration decreased, reaching nearly 99.4% at 10^{-9} M. This concentration-dependent behavior indicates that the Fe/Quasi MOF adsorbent possesses exceptionally high affinity for methylene blue molecules and maintains high activity even at trace concentrations. The observation also suggests that the removal mechanism is not limited by active site availability at lower concentrations, allowing near-complete removal.

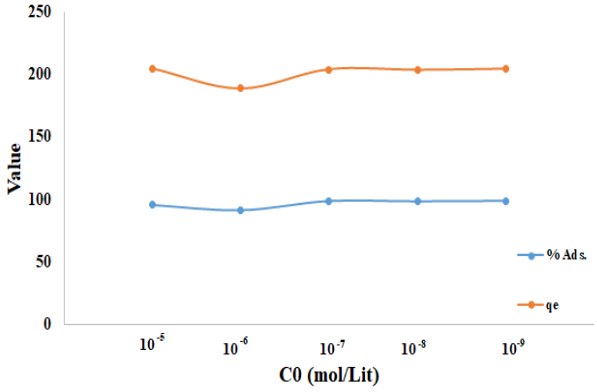

Fig. 9. The effect of different initial concentrations on dye removal from aqueous solution.

GMDH Neural Network Modeling

Optimal Network Architecture

The GMDH-GA algorithm successfully converged to an optimal network architecture comprising three hidden layers with a total of 12 quadratic neurons. The training and testing errors achieved were:

- **Training RMSE:** 0.0043652
- **Testing RMSE:** 0.0068442
- **Overall R^2:** 0.9922

The low testing RMSE (less than 0.007) demonstrates the excellent generalization capability of the developed model, indicating that overfitting did not occur despite the limited dataset size (34 points). The high R^2 value confirms that the model explains more than 98% of the variance in the experimental data.

Sensitivity Analysis

Sensitivity analysis was performed by counting the frequency with which each input variable appeared in the first-layer neurons of the optimal GMDH chromosome. The results are presented in Table 2.

Table 2. Frequency analysis of input variables in the optimal GMDH model

Input variable	Frequency in first layer	Influence rank
Adsorbent dosage (g)	8	1
pH	7	2
Contact time (min)	7	2
Initial concentration (Log M)	6	3
Temperature (°C)	6	3

The frequency analysis reveals that adsorbent dosage exerts the most significant influence on the removal process (8 appearances), followed by pH and contact time (7 appearances each). Initial concentration and temperature have somewhat lower influence (6 appearances each). This ranking is consistent with the experimental optimization results: (i) adsorbent dosage directly determines the number of available active sites; (ii) pH governs surface charge, radical generation, and electrostatic interactions; (iii) contact time determines the extent of dye-adsorbent interaction; (iv) temperature and initial concentration show relatively modest effects within the tested ranges.

Model Validation

Fig. 10 presents a scatter plot comparing the experimental residual dye concentrations with those predicted by the GMDH model. The data points cluster closely around the y = x diagonal line, with no

systematic bias observable across the concentration range. The high correlation coefficient (R^2 = 0.9922) and low prediction error (RMSE = 0.00684) confirm the reliability of the developed model for predicting methylene blue removal efficiency under varying operating conditions.

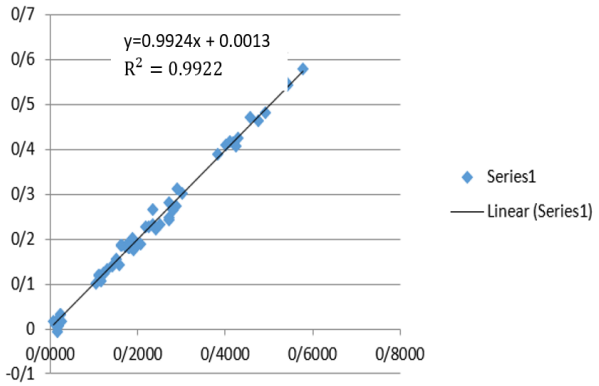

Fig. 10. Comparison of experimental data and modeling output with multi-target GMDH of dye removal by adsorbent

Conclusions

In this study, Fe/Quasi MOF UIO-66 (Zr) nanocomposite was successfully synthesized via an ultrasonic method followed by controlled calcination at 350 °C. Comprehensive characterization using XRD, FTIR, SEM and N_2 physisorption analysis confirmed the formation of the desired quasi-MOF structure with nanoscale dimensions (average crystallite size 73 nm), moderate specific surface area (314.5 $m^2 \cdot g^{-1}$), mesoporous characteristics, and adequate thermal stability up to 400 °C.

Experimental optimization of methylene blue removal revealed that maximum removal efficiency exceeding 96% was achieved under optimal conditions: adsorbent dosage 45 mg, pH 11, initial dye concentration 10^{-9} M, contact time 12 minutes, and temperature 70 °C. The enhanced removal efficiency under alkaline conditions was attributed primarily to favorable electrostatic interactions between the adsorbent surface and methylene blue molecules.

The core contribution of this work is the development of a GMDH-GA hybrid neural network model for predicting residual methylene blue concentration based on five input variables. The optimized model achieved high predictive accuracy (testing RMSE = 0.00684, R^2 = 0.9922) and, through sensitivity analysis based on variable frequency in the optimal chromosome, identified adsorbent dosage (8 repeats) as the most influential parameter, followed by pH and contact time (7 repeats each). This modeling approach provides a valuable analytical tool for predicting process performance under untested conditions without requiring additional costly experiments.

The insights gained from this study—both from experimental optimization and analytical modeling—can guide the design of MOF-based adsorbent systems for wastewater treatment applications. Future work should explore the generalizability of the GMDH model to other dye pollutants and investigate the long-term stability and recyclability of the Fe/Quasi MOF UIO-66 (Zr) adsorbent under continuous operation conditions. On the other hand, although this study focused on model methylene blue solutions to systematically investigate the effects of key parameters, future work will extend the evaluation to real wastewater samples containing competing ions and organic matrices to assess the practical applicability of the Fe/Quasi MOF UiO-66 adsorbent under realistic conditions.

References

[1]. Dhanasekaran, N.C., Water scarcity—challenging the future. ***International Journal of Agriculture Environment and Biotechnology,* 2019**, 12(3), 157–164. DOI:10.30954/0974-1712.03.2019.3

[2]. Tkaczyk, A., Mitrowska, K., Posyniak, A., Synthetic organic dyes as contaminants of the aquatic environment and their implications for ecosystems: A review, ***Science of the Total Environment,* 2020**, 717, 137222. DOI: 10.1016/j.scitotenv.2020.137222

[3]. Ghafoor, S., et al. Evaluation of azo dyes degradation potential of Aspergillus strains: A strategy for waste management, ***Journal of Hazardous Materials Advances,* 2024**, 16, 100475. DOI: 10.1016/j.hazadv.2024.100475

[4]. El-Sayed, E., et al. Azo dyes: Synthesis, classification and utilisation in textile industry, ***Egyptian Journal of Chemistry,* 2024**, 67(4), 221–236. DOI: 10.21608/ejchem.2024.257952.9057

[5]. Alsantali, R., et al. Miscellaneous azo dyes: A comprehensive review on recent advancements in biological and industrial applications, ***Dyes and Pigments,* 2021**, 199, 110050.
DOI: 10.1016/j.dyepig.2021.110050

[6]. Akter, F., Dong, Y., Investigation of removing orange II azo dye from wastewater through an oxidation process, ***Applied Water Science,* 2024**, 14(3), 45.
DOI:10.1007/s13201-024-02105-8

[7]. Al-Tohamy, R., et al. A critical review on the treatment of dye-containing wastewater: Ecotoxicological and health concerns of textile dyes and possible remediation approaches for environmental safety, ***Ecotoxicology and Environmental Safety,* 2022**, 231, 113160.
DOI: 10.1016/j.ecoenv.2022.113160

[8]. Chaabna, I., Delimi, R., Testas, R., Removal of methylene blue using magnetic Na-bentonite composite in aqueous solutions, ***Desalination and Water Treatment,* 2024**, 318, 100353.
DOI: 10.1016/j.dwt.2024.100353

[9]. El-Baz, A., et al. Adsorption technique for pollutants removal; current new trends and future challenges—A review, ***The Egyptian International Journal of Engineering Sciences and Technology,* 2020**, 32(1), 1–24.
DOI:10.21608/eijest.2020.45536.1015

[10]. Zemouri, A.E., et al. Efficient wastewater decontamination using magnetic bentonite-alginate beads: A comprehensive study of adsorption dynamics, regeneration, and molecular interactions, ***Journal of Environmental Chemical Engineering 2024***, 12(3), 113000.
DOI: 10.1016/j.jece.2024.113000

[11]. Das, S., et al. Advanced oxidation processes for dye removal from wastewater: A review, ***Environmental Science and Pollution Research 2024***, 31, 4500–4530.
DOI:10.1007/s11356-024-34567-8

[12]. Furukawa, H., Cordova, K.E., O'Keeffe, M., Yaghi, O.M., The chemistry and applications of metal-organic frameworks, ***Science 2013***, 341(6149), 1230444.
DOI:10.1126/science.1230444

[13]. Hayat, A., et al. Recent advance in MOFs and MOF-based composites: Synthesis, properties, and applications, ***Materials Today Energy 2024***, 41, 101542.
DOI: 10.1016/j.mtener.2024.101542

[14]. Zheng, J., et al. Universal strategy for metal-organic framework growth: From cascading-functional films to MOF-on-MOFs, ***Small 2024***, 20(34), 2305678.
DOI:10.1002/smll.202305678

[15]. Cavka, J.H., et al. A new zirconium inorganic building brick forming metal organic frameworks with exceptional stability, ***Journal of the American Chemical Society 2008***, 130(42), 13850–13851.
DOI:10.1021/ja8057953

[16]. Kandiah, M., et al. Synthesis and stability of tagged UiO-66 Zr-MOFs, ***Chemistry of Materials 2010***, 22(24), 6632–6640.
DOI:10.1021/cm102601v

[17]. Wang, Y.L., et al. UiO-66-based metal organic frameworks for the photodegradation of acetaminophen under simulated solar irradiation, ***Journal of***

Environmental Chemical Engineering, **2021**, 9(5), 106087.
DOI: 10.1016/j.jece.2021.106087

[18]. Zorainy, M.Y., et al. Microwave-assisted synthesis of the flexible iron-based MIL-88B metal-organic framework for advanced energetic systems, ***Journal of Inorganic and Organometallic Polymers and Materials,*** **2022**, 32(4), 1128–1142.
DOI:10.1007/s10904-021-02189-w

[19]. Payam, A.F., Khalil, S., Chakrabarti, S., Synthesis and characterization of MOF-derived structures: Recent advances and future perspectives, ***Small,*** **2024**, 20(15), e2310348.
DOI:10.1002/smll.202310348

[20]. Liu, P., Lyu, J., Bai, P., One-step synthesis of Al-doped UiO-66 nanoparticle for enhanced removal of organic dyes from wastewater, ***Molecules,*** **2023**, 28(5), 2182.
DOI:10.3390/molecules28052182

[21]. Wan, T., et al. Adsorption-photocatalysis for methylene blue dye removal by novel Fe-MOFs through defect engineering, **Journal of the Chinese Chemical Society**, **2024,** 71(11), 1280–1295.
DOI: 10.1002/jccs.202400123

[22]. Hemdan, M., Ragab, A.H., Gumaah, N.F., Mubarak, M.F., Sodium alginate-encapsulated nano-iron oxide coupled with copper-based MOFs (Cu-BTC@Alg/Fe_3O_4): Versatile composites for eco-friendly and effective elimination of Rhodamine B dye in wastewater purification, ***International Journal of Biological Macromolecules,*** **2024**, 274(Pt 2), 133498.
DOI: 10.1016/j.ijbiomac.2024.133498

[23]. Ivakhnenko, A.G., The group method of data handling—A rival of the method of stochastic approximation, ***Soviet Automatic Control,*** **1968**, 13(3), 43–55.

[24]. Fofanah, A., et al. Artificial neural network model with adaptive GMDH technique for non-linear regression prediction, ***International Journal of Scientific & Engineering Research,*** **2021**, 12(4), 1142–1150.
DOI:10.14299/ijser.2021.04.02

[25]. Monshi, A., Foroughi, M.R., Monshi, M., Modified Scherrer equation to estimate more accurately nano-crystallite size using XRD, ***World Journal of Nano Science and Engineering,*** **2012**, 2(3), 154–160.
DOI:10.4236/wjnse.2012.23020

[26]. Katz, M.J., et al. A facile synthesis of UiO-66, UiO-67 and their derivatives, ***Chemical Communications,*** **2013**, 49(82), 9449–9451.
DOI:10.1039/c3cc46105j

[27]. Eltaweil, A.S., et al. Fabrication of UiO-66/MIL-101(Fe) binary MOF/carboxylated-GO composite for adsorptive removal of methylene blue dye from aqueous solutions, ***RSC Advances,*** **2020**, 10(32), 19008–19019.
DOI: 10.1039/D0RA02424D

[28]. Kim, H., et al. Controlling the structural robustness of zirconium-based metal organic frameworks for efficient adsorption on tetracycline antibiotics, ***Water,*** **2021**, 13(13), 1869.
DOI:10.3390/w13131869

[29]. Pu, H., et al. Anchoring Au on UiO-66 surface with thioglycolic acid for simultaneous SERS detection of paraquat and diquat residues in cabbage, ***Microchemical Journal,*** **2023**, 190, 108563.

DOI: 10.1016/j.microc.2023.108563

[30]. Ghalei, B., et al. Rational tuning of zirconium metal-organic framework membranes for hydrogen purification, ***Angewandte Chemie International Edition,*** **2019**, 58(40), 14038–14043.
DOI:10.1002/anie.201907381

[31]. Xu, W., et al. A facile method for preparing UiO-66 encapsulated Ru catalyst and its application in plasma-assisted CO_2 methanation, ***Nanomaterials,*** **2019**, 9(10), 1432.
DOI:10.3390/nano9101432

[32]. Azizi, E., et al. Prediction of groundwater level using GMDH artificial neural network based on climate change scenarios, ***Applied Water Science,*** **2024**, 14(4), 88.
DOI:10.1007/s13201-024-02190-9

[33]. Fallahi, S., Shaverdi, M., Bashiri, V., GMDH-type neural network and genetic algorithm. In: Computational Intelligence in Data Mining, ***Springer,*** **2014**, pp. 267–280.
DOI:10.1007/978-81-322-2205-5_23